‘Cloudbuster’ - A Python-based open source application for 3D reconstruction and quantification of stacked biological imaging samples

A. Rohwedder[1], S. Knipp[2], F.O. Esteves[3], M. Hale[3], S.E. Ketchen[1], D. Treanor[3,4,5,6], A. Brüning-Richardson[2]

Address:

1 Light Laboratories, School of Molecular and Cellular Biology, University of Leeds, Leeds, UK

2 School of Applied Sciences, University of Huddersfield, Huddersfield, UK

3 Leeds Institute of Cancer and Pathology, University of Leeds, Leeds, UK

4 Leeds Teaching Hospitals NHS Trust, Leeds, UK

5 Department of Clinical Pathology, and Department of Clinical and Experimental Medicine, Linköping University, Linköping, Sweden

6 Center for Medical Image Science and Visualization (CMIV), Linköping University, Linköping, Sweden

Corresponding authors:

Dr Arndt Rohwedder: arndt.rohwedder@mail.de

Dr Anke Brüning-Richardson: a.bruning-richardson@hud.ac.uk

Abstract

Three dimensional (3D) spheroid cultures are generating increasing interest in cancer research, e.g., for the evaluation of pharmacological effects of novel small molecule inhibitors. This is mainly due to the fact that such 3D structures reflect physiological characteristics of tumours and the cellular microenvironments they reside in more faithfully than 2D cell cultures; in addition, they allow the reduction of animal experiments whilst providing significantly relevant human-based models. Quantification of such organoid structures as well as the mainly slice-based acquisition and thus forced 2D representation of 3D spheroids provide a challenge for the interpretation of the associated generated data. Here we provide a novel open source workflow to reconstruct a 3D entity from slice recorded microscopical images with or without treatment with anti-migratory small molecule inhibitors. This reconstruction produces distinct point clouds as basis for subsequent comparison of basic readout parameters using average computer processor, memory, and graphics resources within an acceptable time frame.

We were able to validate the usefulness of this workflow using 3D data generated by various imaging techniques, including z-stacks from confocal microscopy and histochemically labelled spheroid sectioning, and demonstrate the possibility to accurately characterise inhibitor effects in great detail.

Keywords: 3D spheroids, 3D imaging, point cloud quantification, glioblastoma, migratory inhibitors, open source

Introduction

Three dimensional (3D) spheroid or organoid cell cultures are becoming increasingly relevant for applications in pharmaceutical, developmental and cancer studies (Hoarau-Véchot et al 2018, Ravi et al 2015, Rios de la Rosa et al 2018). It is generally acknowledged that the development of these systems is driven by the possibility to recreate physiologically accurate cell micro-environments and, in the case of cancer studies, 3D structures resembling tumour morphology (Wang et al. 2009). Additionally, with increasing demands to reduce animal experiments in pre-clinical studies, these techniques also provide controlled conditions comparable to traditional two dimensional (2D) cell cultures (Vorrink et al. 2018). This development coincides with the development of increasing numbers of cost effective and high-speed 3D imaging systems.

Unlike 2D cell cultures, a 3D spheroid culture generates additional conditions that cannot be recapitulated in 2D. The most striking features include the creation of hypoxic regions in the centre of a spheroid and cell-cell contacts in any possible direction, forming potential barriers (Kim et al. 2011). Under these conditions the accessibility of drugs and inhibitors to individual cells in 3D cell cultures generates valid testing platforms for research and pharmacology. However, one drawback of these assays is the difficulty to generate quantifiable and meaningful readouts associated with such higher dimension and complexity (Costa et al. 2016). This is partly due to the greater effort of growing and then recording 3D cell cultures especially for live cell imaging, but also the necessity to analyse a 3D spheroid as an intact entity. While software exists to analyse 3D structures, a unifying approach that allows the analysis of spheroids from different acquisition sources in a time and computational resource efficient manner is urgently required. This is caused in part by the application focus of the applied imaging platform. For example, whilst a confocal microscope resolves internal structures at the sub-cellular level effectively, a lightsheet microscope is the method of choice for global (whole mount) structures. This provides already problems to compare 3D images derived from these two platforms. Most microscopy-based acquisition systems record 3D images by scanning slice wise in z-dimension. This results in a stack of individual 2D images, often with differing xy-z dimensional resolutions. Excellent freely available and adaptable software exists for the analysis of the morphology of individual slices, i.e., NIH ImageJ, Fiji, Volocity, but remain problematic for analysing whole 3D structures as such. This becomes evident when considering quantification of cellular structures spanning several slices in an image stack. Cell extensions or cell structures such as filopodia originating from different slices would be treated as isolated entities and thus quantified separately due to their first and last

appearance in different slices. This leads to an incorrect description of the object under observation. Much computational effort is necessary to correct resulting data for 3D. Commercially available software for (biological) microscopical imaging samples is not only often expensive but due to its closed source nature does not allow adaptation or verification of the used algorithms. These two factors strongly limit the usability of this type of software in academia. On the other hand, free and extensible software for the preparation and analysis of 3D structures exists (i.e., CloudCompare, Meshlab) that do not utilize image stacks but point cloud data for analysis. This type of software usually originates from a technical or geographical background, where 3D data sets are readily available and used (Ayman et al. 2005, Torregrossa et al. 2011).

To address the mentioned drawbacks, we developed a novel workflow, which allows the transformation of a variety of microscopically generated data, such as scanned histopathological microtome sections or confocal z-stacks of microscopically recorded glioma spheroids, into single 3D point cloud structures in combination with morphological analysis. To further evaluate the newly developed workflow, glioma spheroids were treated with various small molecule inhibitors targeting different cellular structures to prevent cell migration. Spheroids were generated from the established glioma cell lines U251 and U87 that have been demonstrated to possess highly migratory activity in previous studies and represent a cancer type that is known to be highly aggressive due to its invasive potential (Ponten & Westmark, 1978).

We were able to obtain meaningful 3D data, such as fragmentation, i.e., the amount of separate 3D structures (like cells or different sized aggregates), dimensional ratios and average distances, and to identify distinct 3D morphologies between different treatments from the reconstructed spheroid structures with our freely available software that can be used on an average PC with most common operating systems (Linux, Windows, Mac).

Methods

Spheroid generation

The glioma cell lines U251 and U87 were grown in vitro as previously described (Ketchen et al. 2020). Spheroids were generated from the cells in low adherent 96-well plates (Nunc, UK) as previously described (Cheng et al ,2015), embedded in collagen and treated with a panel of small molecule inhibitors at predetermined anti-migratory concentrations, including 6-bromoindirubin-3-oxime (5 μM) (BIO, Selleckchem), latrunculin

A (10 μM) (lat A, Tocris), and CCG-1423 (500 nM) (Tocris). Glioma cells emanating away from the original spheroid cores were allowed to migrate into collagen for 72 hours. After completion of the experiment the whole collagen plugs containing spheroids and migrating cells were fixed with PFA (4% in PBS, overnight at 4°C).

Confocal microscopy

For confocal microscopy, spheroids and migrating cells within collagen plugs were permeabilised with PBS-Tween (0.5%) and labelled with ActinRed (ThermoFisher). Fluorescently labelled samples were imaged on a Zeiss LSM 880 AxioObserver confocal microscope using (Carl Zeiss) using an EC Plan-Neofluar 10x/0.3 objective.

Lightsheet microscopy

Hek293 cells were transfected with FGFR2-GFP vector as previously reported (Ahmed et al. 2013) and grown in agarose covered round bottom 96 well plates (Nunc) in DMEM (Gibco) containing 10% FCS (ThermoFisher) and 1% penicillin and streptomycin (ThermoFisher). Upon reaching a size of approximately 1mm, spheroids were trapped in low melting agarose (Biorad) and transferred in a 1ml syringe with the outlet cut off on a specimen holder. Lightsheet images were recorded on an AxioObserver SPIM microscope (Carl Zeiss) with Plan-Apochromat 20x/1.0 UV-VIS objective, 488 Laser excitation, AIMApplication software.

iSIM imaging

The iSIM used for this study was home-built at the University of Leeds (Curd et al 2015). The objective lens used was a ×60/1.2 objective (Olympus). Z-stacks from U251 cells (labelled with Alexa Fluor 488 phalloidin at 1/500 (Molecular Probes, Invitrogen, USA) and anti-acetylated tubulin antibody (1/500) with Alexa Fluor 594 pre-adsorbed (1/500; Molecular Probes, Invitrogen, USA)) embedded in rat tail collagen V (Corning Life Science, USA) were acquired at 50 ms per slice as described in Ketchen et al. (2020). Deconvolution was performed on all final images using the ImageJ plugin DeconvolutionLab (Biomedical Imaging Group, EPFL, Switzerland).

Histochemistry

Paraffin embedded spheroids and associated migratory cells (suppl. figure 1A) were generated as previously described (Cheng et al, 2015) and serially sectioned at 5µm on a rotation microtome. Approximately 50 slides per sample were stained using H&E for reconstruction of the whole spheroid and surrounding migratory rim (suppl. figure 1B). Slides were scanned using Aperio digital scanners at 20x magnification at the University of Leeds. (suppl. figure 1C).

3D reconstruction of microtome slices

Single scanned images of spheroid sections were sorted according to the order they had been sectioned and stained and then cropped using Fiji. An image stack was built and the orientation of the single image toward each other was adjusted using the Fiji registry plugin: Align image by line ROI. Missing slices were replaced by copies of previous slices. Resulting stacks were saved as tiff files.

Python workflow

The python based workflow developed as part of this work transforms slice based 3D images (e.g., confocal xyz-stacks) into a point cloud structure and delivers a basic quantification of the spheroid (figure 1). One of the main objectives has been the reduction of bias, providing an automatism with very limited user interference. The workflow can be run in single file analysis or in bulk analysis for multiple files in one run. Here only the single file analysis has been used.

As a prerequisite the workflow requires a grey scale 3D image stack in TIF file format. In the single file analysis mode, the user is required to enter the pixel dimensions in all three directions (suppl. figure 3A) in the GUI and to choose the background color (white or black). When done, the regarding file to analyse must be loaded by a file selector. The analysis starts as soon as the OK button is pressed. In case of bulk analysis, a script file containing the same data needs to be provided and the analysis starts upon loading the script file. If a TIF file containing metadata exists, the script file can be generated automatically.

Figure 1 supplies an overview on the modules used during the analysis process. In a first step the *fileselector* from the *wx* module is used for selecting the file to be analysed and

the associated user entries (figure 1, white boxes). The file then is loaded into memory using the *io* module from *skimage*. From X/Y/Z resolution entries the axis ratios are calculated.

Based on the calculated axis ratios the software first extrapolates the initial image stack (suppl. figure 2A) to a 3D stack with even dimension ratios using the python *skimage* module function *transform.rescale* (figure 1, 1. blue box; suppl. figure 2B). Using *skimage.draw* an additional frame in the background color is drawn around the perimeter of the stack to provide a closed structure. It then applies a transformation to a binary stack, performed by the python *skimage* module *filters*, with the *threshold_li* function (Sezgin & Sankur 2004) (figure 1, 2-3. blue box; suppl. figure 2C). To reduce data volume for the analysis a *skimage* edge detection algorithm (figure 1, 4. blue box; Canny, 1986) is applied, where the original stack matrix is rotated twice with the *transpose* function of the *numpy* module to cover the surface as completely as possible. Using the function *canny* of the *skimage* module *feature* the with the *numpy.where* function extracted edge positions of all three dimensions are combined to a single array (figure 1, 1. green box). Redundant points are removed from the array with the *numpy* module function *unique* (figure 1, 2. green box), and the result is saved as a point cloud in PLY format with the *open3D io* module (Zhou et al 2018) (figure 1, 1. yellow box; fig. 2 a-b, suppl. 2 d-e, 3c).

The *open3D* module is also used for quantification of the resulting point cloud. In detail:

Apart from the overall point cloud size using the *get_max_bound* function (figure 1, 2. yellow box), the *cluster_dbscan* function allows to fraction and label individual spheroid elements. This has been used to split the original point cloud in smaller parts (i.e., cells or smaller spheroids) while preserving the individual positions. From size calculations of the maximum bounds the largest resulting cloud then has been declared as central spheroid. The function *compute_point_cloud_distance* is used to calculate the distance of the smaller isolated point clouds to the central spheroid (figure 1, 3. yellow box). The previous isolated central sphere is further processed to also extract information on the shape. An ellipsoid shape is fitted to the central spheroid using the gradient descent method, transformed into a point cloud using *utility.Vector3dVector* from the *open3D* module and then subtracted by excluding all points enclosed in the ellipsoid from the original spheroid. The same procedure as for the identification of the fractionation for the entire point cloud is then applied on the remaining point cloud data, providing the measurements for the extensions (figure 1, 4. yellow box).

Intermediate results are individually saved for further investigation. Beside the complete translated image stack stored as a point cloud this includes colour coded separated

fragments (like isolated cells/accumulates), the isolated largest, thus central spheroid, the adapted ellipsoid, and the isolated extensions in point cloud format (.ply), respectively. The numeric results are stored with the addition of "_Final_Results.csv" to the original filename in comma separated value format.

This specialised python script bridges the gap between slice based image analysis and 3D based entity analysis while avoiding the need of extensive background knowledge from the user. The handling of the script via its GUI is therefore straight forward, resulting in the swift generation of indicative data for evaluation. This is demonstrated by the example on the effect of drug activity on cell migration in 3D spheroids. Accessibility of intermediate steps allows the usage for further in depth analysis and, in the case of point cloud PLY files, opens the analysis via already existing sophisticated technical software.

Additional to a single image stack mode as presented here, the script can be run in batch mode with data analysis for higher data volumes, using the *sklearn* python module. We named the developed script 'Cloudbuster.'

The source code can be downloaded at:
https://github.com/ARRohwedder/Cloudbuster

Results

The 'Cloudbuster' script

Cloudbuster is a collection of python scripts, combined via a common menu script. Either single stack analysis or a script based analysis of multiple stacks is possible. The results can be analysed in the data analysis part, providing an overview of possible relations between the analysed samples. Central to the package is the single stack analysis part on which also the analysis of multiple image stacks relies. Here, we will only present data derived from single stack analysis to demonstrate Cloudbuster's versatility to analyse image data from diverse sources.

The script combines several freely available python modules to enable a transformation from slice based image stacks to point cloud data for 3D data analysis. The most important python modules for this very process are: Open3D and skimage.

To avoid necessity of major user interference, thus avoiding inadvertent bias and therefore providing experimental comparability, only basic information input by the user is required to start analysis of tif-stacks, regardless of image source and size. Basically, only stack

calibration data, i.e., X/Y/Z resolution, background color (black/white) and file name are required to start the analysis. Upon pressing the start button the target stack can be chosen and the software starts 3D transformation and analysis of the image data. Quantification data and 3D reconstructions are stored during this process in the original tif-stack folder.

The workflow also allows for a batch analysis of multiple image stacks without the requirement to load image stacks individually. A short script file including image stack names and calibration data is sufficient to start analysis of multiple stacks without further user interference. When calibration data are stored as meta-data in the respective image stacks the script file can be generated automatically using the script maker part of the Cloudbuster workflow.

Dedicated to the analysis of multiple image stacks the workflow includes an additional data analysis part that performs data analysis of quantification data using the python modules PCA and Sklearn.

Point cloud 3D spheroid reconstruction from IHC sections

To demonstrate the quantification capabilities of the workflow, histologically prepared U251 spheroids treated with different anti-migratory inhibitors were used. Strikingly, reconstruction of 3D point cloud structures with Cloudbuster from individual slices of untreated U251 or inhibitor-treated spheroids revealed already distinct morphologies depending on the treatment by visual inspection alone (figure 2A). The untreated U251 spheroid displayed a seemingly uniform and directional spread of cells away from the central spheroid while all inhibitor treated spheroids appeared to be more ‘compacted’, i.e., confined to the borders of the central spheroid. Treatment with different inhibitors appeared to result in different degrees of ‘compactness.’ The lat A treated spheroid appeared to be the most restrained, whereas CCG-1423 and BIO induced a similar phenotype but revealing some emerging cellular extensions away from a central region, though less pronounced as observed for the untreated spheroid (figure 2A, blue, yellow). However, we conclude that on the basis of observation only, a quantitative differentiation between the spheroids under investigation is inadequate.

Quantification of the overall shape

A crucial part of this workflow is the identification and quantification of easily accessible

indicators for the evaluation of 3D microscopical objects, like spheroids. Cloudbuster calculates 24 indicative values from each object (sup table 1). Here we concentrated on the six most prominent parameters between the treatments that were subsequently fully integrated into the software workflow (figure 1 and figure 3A-F). Six programmatically and easily accessible indicators were: the *extensions of the structure bounding box* in the form of Y/X (*length/width*) and X/Z (*width/height*) direction ratios, *the structural fragmentation number*, *point distance from the central sphere, number of extensions and average length of extensions*, respectively. All values are partly independent of calibration or based on neutral pixel values for comparison purposes.

The *bounding box Y/X - X/Z axis* ratios (figure 2A, figure 3C) were able to identify the directional deviation of the spheroid in 3 dimensions. Furthermore, the *Y/X* ratio has the potential to obtain information of a directed cellular migration / polarisation for central spheroid growth from the central spheroid (figure 3C). A value deviating from 1 represents a “stretched” spheroid, thus extending in one direction, unlike a “round” spheroid which would result in a value of 1. Additional experimental information would be necessary to yield angular information from the above ratio. By providing intermediate point cloud results these data can be used to produce representative 3D graphics using, for example, meshlab (figure 2 A,C,D,F,G). Though the presented experiments did not uncover noticeable differences in the Y/X ratio in general, the BIO treated spheroid stands slightly out in approaching level extension in X and Y axis by converging towards the value 1 (0.98), indicating no planar directionality.

The *X/Z* ratio would allow for a further different characterisation of the individual spheroids (figure 3D). Higher values of this index indicate more flattened structures and therefore more horizontally/planar spread spheroids. In our experiments the highest value was generated for the spheroid in untreated condition (1.77). This value confirmed the expectations from the graphical point cloud meshlab representation of combined investigated histological spheroids in figure 2A where the untreated spheroid clearly appeared “flatter” than the inhibitor treated. It was not easy to distinguish the different inhibitor treated spheroids by eye. However, crucially the X/Z ratio allowed comparison of the structures and revealed that the BIO treated spheroid presented itself structurally as the closest to a Z-plane extended sphere (0.67).

Quantification of cellular dissemination

The newly developed workflow allowed to generate a central ellipsoid with a minimal radius of half the minimum bounding box extension (figure 2B,C). This ellipsoid

represented an ideal shaped spheroid as a reference for migration-related events. Calculations of the average distance of points outside the central ellipsoid revealed a marked difference between untreated and inhibitor treated spheroids (figure 3A). This indicator supports the optical impression of different morphological appearances. The high value (388.18 µm) obtained in the case of the BIO treated spheroid suggests strong deviation from the ideal ellipsoid, compared to strikingly lower values in the other treated and untreated spheroids (Latrunculin A = 120.84 µm; CCG = 171.77 µm; Medium = 181.05 µm). Lower average distance values imply slower spreading cells from the central sphere, provided an approximately equal start and growth time. The higher value in the BIO treated spheroid therefore suggests the uncontrolled migration away from the centre and apparently contradicts the shape data. However, the impression in the 3D representation (figure 2A) seemingly confirm the data. Due to extensions in all planar directions a defining box necessarily approaches the value of 1 in the Y/X ratio.

Quantification of spheroid fragmentation

Spheroid shape and the average distance to the central ellipsoid appear to contradict the “reduced” impression of the BIO treated spheroid in figure 2A compared to the untreated spheroid. The fragmentation of structure provides conclusive data for the evaluation of the treatment effects. This indicator counts the number of isolated particles, including the central spheroid, beyond a certain threshold (>10 adjacent vertices).

The differences in the number of fragments (cells) in between inhibitor treated spheroids (80-220) were strongly overshadowed by the count in the untreated spheroid (707). The structural fragmentation of the point cloud was performed by segmentation on the basis of relational distance, or clustering (figure 3B). In the presented experiments the highest value was found in the untreated spheroids, indicating a high number of individual components. Those components differ in size, from single cells to extended clusters. The number allows to interpret migratory activity within the analysed structure. When inhibitor treated spheroids were compared separately this indicator showed remarkable differences. By far the lowest value was found for the BIO-treated spheroid (80), closely followed by the lat A treated spheroid (110).

Fragmentation of structure can be considered as a readout for the metastatic capabilities of the spheroid under observation. Higher numbers in this parameter represent higher numbers of potential new nucleation points for spheroids. Confirmation from *in vivo* studies would be necessary for verification.

Quantification of spheroid extension

Extensions are defined as parts connected to the spheroid point cloud but exceeding the limits of a calculated fitted central ellipsoid. The workflow subtracts the ellipsoid and quantifies the number and size of the remaining extensions (figure 3E,F).

Application to the histologically prepared U251 spheroids lead to the highest count of extensions for the untreated/medium treated spheroids (110) (fig. 3E).

The workflow further allows to distinguish between different treatments, with lat A as the treatment with strongest reduction in the number of extensions (25), while CCG and BIO treatment both generated lower numbers of extensions compared to the ones found in the medium treated spheroid (69, 53); however, these inhibitors still induced higher numbers than those seen in the lat A treated spheroids. Quantification of the extension lengths failed to generate remarkable differences apart from BIO, which stands out compared to the other analysed spheroids. Calculated average extension lengths for medium (84.90 µm), lat A (60.94 µm) and CCG (62.78 µm) were remarkably shorter than BIO treated spheroids (121.33 µm) (figure 3F).

It has to be pointed out that the results are limited to the measurement of one single spheroid each and are shown here as proof of principle to represent the differential capabilities of the workflow quantifications. Nevertheless, the listed observations present intriguing insights in the response of U251 spheroids to the treatment with inhibitors targeting cell migration.

To summarise, the quantification data, careful evaluation allows the characterisation of the untreated spheroid as highly migratory/invasive, in terms of isolated cells and extensions. This accounts for a highly metastatic potential. While all inhibitors target migration and invasion, the most effective appears to be BIO in terms of fragmentation of structure and roundness (Y/X ratio and X/Z ratio).

Versatility of the software to analyse different image data sources

a. Confocal imaging

Confocal image stacks of individual U87 spheroids embedded in collagen were obtained at different timepoints (t= 24h and t=48h) and the stacks were added to the Cloudbuster workflow. A difference in values obtained for the parameters was expected between growth/migration periods of 24 hours and 48 hours, respectively. Visually, an apparent

increase in spheroid size was observed (figure 4A). In addition, parameters derived from the quantification revealed an increase in the number of separated components (cells or aggregates) and the distance migrated from the central spheroid. Finally, the number and length of extensions emanating away from the spheroids had increased over time as determined by data analysis (figure 4B).

b. iSIM imaging

As proof of principle of applicability of the software to data generated by different means, we also tested Cloudbuster on an image stack generated by iSIM imaging. An uncalibrated .tif stack was added to the workflow (figure 4C,D). Due to the reduced scale of the image stack compared to the reconstructed microscopical slices mentioned earlier we noted that analysis was performed much quicker (approx. ½ time). Stored resulting point clouds and quantification (figure 4E) performed as expected and an appropriate point cloud model was stored (figure 4D).

c. Lightsheet imaging

Lightsheet imaging tends to generate much larger data volumes than conventional or confocal microscopic imaging. We therefore tested the Cloudbuster workflow on a partial scan of a larger Hek293 spheroid (figure4 F, G). Although performing without any runtime error and producing an adequate point cloud (figure 4G), the resulting data were not as expected (figure 4H). Especially ‘ellipsoid fitting’ did not perform convincingly. The ellipsoid (light green, figure 4C) appears to be partly rotated out of the spheroid boundaries (red and grey, figure 4C). However, closer inspection of the generated point cloud model revealed a flat cut plane on one side of the spheroid, caused by the partial scan. This resulted in a flattened plane on one side of the spheroid instead of a complete spheroid during acquisition, thus corrupting the resulting data for analysis.

Discussion

With demand for precision medicines and treatments it has become increasingly clear that traditional 2D cell cultures have a limited applicability in drug screens (Koledova, 2017). The move toward 3D cell cultures and associated screens in a 3D environment has been hampered by the lack of associated software allowing the accurate recording, normalisation and interpretation of data generated in 3D. In addition, the computational complexity of 3D structures results in huge datasets leading to problems associated with

time to analyse and eventually store data. Here, we attempted to circumvent these problems without the requirement for memory consuming closed source and expensive commercial products like Volocity® (Perkin Elmer®) or MetaMorph® (Molecular Devices®). Both softwares provide a high number of analysis opportunities but require powerful computers with associated costs and unknown algorithms; in addition, they are designed for a more general purpose including data generated in 2D and therefore are not equipped to provide quick results for data sets generated by various means in from 3D structured and examined in a 3D environment.

Commercially available software like Volocity is limited to Windows or, in the case of Imaris® (Oxford instruments®) Mac and Windows. Also, as closed source software commercial software does not allow insight into the algorithms used, resulting data can be considered disputable and cannot be adapted to personal needs. By using the freely available interpreter language the novel workflow 'Cloudbuster' presented here is designed to be used on average PC platforms, independent of the installed operation system. The open source nature of the workflow also allows user specific adaptations.

Requiring only limited user knowledge (original X/Y/Z resolution, light/dark background, filename) the Cloudbuster workflow performs quantification of sliced image data from a broad range of sources. The Cloudbuster scripts allow the retrieval of indicative quantification values for a detailed and concise 3D interpretation of spheroids and associated migratory cells. As proof of principle, we used 3D reconstructed sliced or z-stacked glioma spheroids subjected to different inhibitor treatments which provided an excellent opportunity to identify highly informative morphological descriptors without the requirement for extensive 3D computational effort. In the presented examples the overall time necessary to analyse a 3000x3000x53 stack required only five minutes on a standard Linux PC, including the documentation of intermediate steps in the shape of individual point cloud files. None of the commercially available software could even be installed on this type of PC (AMD Athlon dual core 2.5 GHz, 16Gb memory, Nvidia Geforce GTX 1650, Ubuntu 20.04.3 LTS).

For our examples, the six most prominent identified key-descriptors (*Av. Point dist. To sphere*, *Fragm. Of struct.*, *X/Y ratio*, *Z/Y ratio, number of extensions, av. Length of extensions*) were able to characterise and interpret the effect of different inhibitors on spheroid and migrating cell morphologies. While all six descriptors were in agreement with the observation that under untreated (control) conditions high migratory activity is detectable, differentiation between the inhibitors was made possible especially by two of the descriptors, *Fragm. Of struct.* and *Av. Number of extensions*. Using the descriptor data

from the workflow it was feasible to morphologically discriminate the effect of the used inhibitors. BIO can therefore be identified as the most effective inhibitor in our experiment in terms of the reduction of spheroid ratios (X/Y ratio, Z/Y ratio) and spreading (Fragm. Of struct). The structural fragmentation and the Z/Y extension descriptors indicate an even higher efficiency than the actin polymerisation effecting latrunculin A. Especially the low fragmentation index (80, compared to Medium = 707, Lat. A = 110 and CCG = 220) is indicative for low invasiveness of the treated spheroid. The data from these experiments demonstrate that single factors can be misleading. From the perspective of the Y/X ratio alone BIO treatment (0.99) and 'medium' treatment (1.05) are very similar. The differences become obvious when including the fragmentation of structure (medium = 707, BIO = 80) and number of extensions (medium = 110, BIO = 53). Finally, the length of those extensions may explain the similarity of both treatments in terms of the Y/X ratio: while untreated spheroids provided comparative short extensions on average (84.9 µm), BIO treated spheroids homolaterally extended on average further (121.33 µm) from the central ellipsoid.

BIO is an inhibitor that targets the activity of Glycogen synthase kinase-3 (GSK-3). GSK-3 is a serine threonine kinase which is involved in many cellular processes in glioma cells including cell migration (Chon et al. 2015). Even though this inhibitor has been the basis of many studies to target cell migration (Yu & Zhao, 2016, Zhao et al. 2019) its mode of action via GSK-3 regulation is still not known, especially in 3D spheroids.

Here, for the first time we were able to demonstrate that BIO not only reduces the migrational activity of single cells away from the central spheroid but results in a more rounded spheroid than any other investigated treatment. Further experiments will be necessary to determine whether the latter only represents the initial state of the spheroid or is the result of the BIO treatment. In contrast, latrunculin A is known to target cell migration by inhibition of actin polymerisation (Oliveira et al. 1996). Again, we were able to differentiate between the two inhibitors by the effect on cell migration in 3D. Latrunculin A not only limits the fragmentation, i.e., migration of single cells, but in contrast also prevents generation of extensions overall. CCG-1423 is a newly developed inhibitor of SRF-mediated transcription activated by Rho pathway signaling (Evelyn et al, 2016). We recently reported on the effect of CCG-1423 on cell morphology in single cell migrating in a 3D environment promoting the switch from a mesenchymal to amoeboid morphology (Ketchen et al, 2020). Here, although the inhibitor CCG-1423 clearly induced morphological changes in the spheroid in comparison to the control, its effect on fragmentation and extension reduction appeared to be the least prominent among all

inhibitors used in this experiment in terms of preventing cell migration, which is in keeping with observations from our more traditional invasion assays (Ketchen et al, 2020).

The Y/X ratio did not generate very differential data in these experiments. This, in combination with the other data, is useful information in itself. Since all our other data on number and size of extensions and single cells/aggregates support our observation of migratory activity, the lack of strong X/Y data indicate non-directional migration, but rather a uniform spreading of cell in all directions. A directed migration would have resulted in a ratio related to either the X or the Y being dominant (i.e., markedly higher, or lower than the value 1).

The presented data here can be generated on an ordinary day- to- day use computer within minutes. The obvious capability of the descriptors to quickly identify even subtle differences between 3D spheroid structures and appendages renders this analysis ideal for large scale analysis of spheroid data. Quantification of 3D structures from different imaging technologies, as demonstrated here, allows the comparison of data from different sources. The 'Cloudbuster' workflow also includes a high throughput and data analysis mode, not covered here. This feature additionally simplifies acquisition and interpretation of imaging data.

Author contributions: Study design: AR, SK, ABR; Methodology: AR, SK, FOE, MH, SK, DT, ABR; Drafting of manuscript: AR, SK, DT, ABR; Final draft review: AR, SK, FOE, MH, SK, DT, ABR

Acknowledgement

We would like to thank Sally Prior for extensive testing of the software and helping to provide the cross-platform applicability of the Cloudbuster workflow.

Data accessibility: The authors are happy to share data on request.

We would like to thank the IBIN network for funding of this work (Award reference IBIN3ABR).

References

Koledova Z. 3D Cell Culture: An Introduction. Methods Mol Biol. 2017; 1612:1-11. doi:

10.1007/978-1-4939-7021-6_1. PMID: 28634931.

Ketchen S, Rohwedder A, Knipp S, Esteves F, Struve N, Peckham M, Ladbury JE, Curd A, Short SC, Brüning-Richardson A. A novel workflow for three-dimensional analysis of tumour cell migration. Interface Focus. 2020 Apr 6;10(2):20190070. doi: 10.1098/rsfs.2019.0070. Epub 2020 Feb 14. PMID: 32194931; PMCID: PMC7061943.

Hoarau-Véchot J, Rafii A, Touboul C, Pasquier J. Halfway between 2D and Animal Models: Are 3D Cultures the Ideal Tool to Study Cancer-Microenvironment Interactions? Int J Mol Sci. 2018 Jan 18;19(1):181. doi: 10.3390/ijms19010181. PMID: 29346265; PMCID: PMC5796130.

Qian-Yi Zhou, Jaesik Park, Vladlen Koltun: Open3D: A Modern Library for 3D Data Processing. ArXiv:2018; 1801.09847

Canny J. A computational approach to edge detection. IEEE Trans Pattern Anal Mach Intell. 1986 Jun;8(6):679-98. PMID: 21869365.

Sezgin M. and Sankur B.: Survey over Image Thresholding Techniques and Quantitative Performance Evaluation. Journal of Electronic Imaging, 2004; 13(1): 146-165 DOI:10.1117/1.1631315

Habib A, Ghanma M, Morgan M, Al-Ruzouq R: Photogrammetric and Lidar Data Registration Using Linear Features. Photogrammetric Engineering & Remote Sensing, 2005; Number 6, pp. 699-707(9)

Torregrossa D, Peyraut F, Fahimi B, M'Boua J, Miraoui A: Multiphysics Finite-Element Modeling for Vibration and Acoustic Analysis of Permanent Magnet Synchronous Machine. IEEE Transactions on Energy Conversion, 2011; Volume: 26, Issue: 2: 490 - 500)

Wang W, Itaka K, Ohba S, Nishiyama N, Chung UI, Yamasaki Y, Kataoka K. 3D spheroid culture system on micropatterned substrates for improved differentiation efficiency of multipotent mesenchymal stem cells. Biomaterials. 2009 May;30(14):2705-15. doi: 10.1016/j.biomaterials.2009.01.030. Epub 2009 Feb 12. PMID: 19215979.

Vorrink SU, Zhou Y, Ingelman-Sundberg M, Lauschke VM. Prediction of Drug-Induced Hepatotoxicity Using Long-Term Stable Primary Hepatic 3D Spheroid Cultures in Chemically Defined Conditions. Toxicol Sci. 2018 Jun 1;163(2):655-665. doi: 10.1093/toxsci/kfy058. PMID: 29590495; PMCID: PMC5974779.

Kim JW, Ho WJ, Wu BM. The role of the 3D environment in hypoxia-induced drug and apoptosis resistance. Anticancer Res. 2011 Oct;31(10):3237-45. PMID: 21965731.

Costa EC, Moreira AF, de Melo-Diogo D, Gaspar VM, Carvalho MP, Correia IJ. 3D tumor spheroids: an overview on the tools and techniques used for their analysis. Biotechnol Adv. 2016 Dec;34(8):1427-1441. doi: 10.1016/j.biotechadv.2016.11.002. Epub 2016 Nov 11. PMID: 27845258.

Ravi M, Paramesh V, Kaviya SR, Anuradha E, Solomon FD. 3D cell culture systems: advantages and applications. J Cell Physiol. 2015 Jan;230(1):16-26. doi: 10.1002/jcp.24683. PMID: 24912145.

Rios de la Rosa J M, Wubetu J, Tirelli N and Tirella A: Colorectal tumor 3D in vitro models: advantages of biofabrication for the recapitulation of early stages of tumour development. Biomedical Physics & Engineering Express, 2018, Volume 4, Number 4

Ponten J and Westermark B: Properties of human malignant glioma cells in vitro.
Med Biol. 1978 Aug;56(4):184-93. PMID: 359950.

Cheng V, Esteves F, Chakrabarty A, Cockle J, Short S, Brüning-Richardson A. High-content analysis of tumour cell invasion in three-dimensional spheroid assays. Oncoscience. 2015 Jun 14;2(6):596-606. doi: 10.18632/oncoscience.171. PMID: 26244167; PMCID: PMC4506363.

Evelyn C R, Lisabeth E M, Wade S M, Haak A J, Johnson C N, Lawlor E R, Neubig R R: Small-Molecule Inhibition of Rho/MKL/SRF Transcription in Prostate Cancer Cells: Modulation of Cell Cycle, ER Stress, and Metastasis Gene Networks.
Microarrays (Basel). 2016 May 28;5(2):13. doi: 10.3390/microarrays5020013.

Oliveira CA, Kashman Y, Mantovani B. Effects of latrunculin A on immunological

phagocytosis and macrophage spreading-associated changes in the F-actin/G-actin content of the cells. Chem Biol Interact. 1996 Mar 25;100(2):141-53. doi: 10.1016/0009-2797(96)03695-2. PMID: 8646787.

Chon E, Flanagan B, de Sá Rodrigues LC, Piskun C, Stein TJ. 6-Bromoindirubin-3'oxime (BIO) decreases proliferation and migration of canine melanoma cell lines. Vet J. 2015 Aug;205(2):305-12. doi: 10.1016/j.tvjl.2014.07.012. Epub 2014 Jul 31. PMID: 25130776; PMCID: PMC4312555.

Yu AS, Zhao L. Effects of the GSK-3β inhibitor (2Z,3E)-6-bromoindirubin-3'-oxime upon ovarian cancer cells. Tumour Biol. 2016 Apr;37(4):4857-64. doi: 10.1007/s13277-015-4344-8. Epub 2015 Nov 2. PMID: 26526575.

Zhao XE, Yang Z, Gao Z, Ge J, Wei Q, Ma B. 6-Bromoindirubin-3'-oxime promotes osteogenic differentiation of canine BMSCs through inhibition of GSK3β activity and activation of the Wnt/β-catenin signaling pathway. An Acad Bras Cienc. 2019 Mar 21;91(1): e20180459. doi: 10.1590/0001-3765201920180459. PMID: 30916158.

Harmer JH, Lolait SJ, Toh BH, Pedersen JS, Chaponnier C, Gabbiani G. Actin depolymerizing factor and the organization and distribution of actin in astrocytomas and meningiomas. *Br J Cancer*. 1983;48(1):89-93. doi:10.1038/bjc.1983.161

Curd A, Cleasby A, Makowska K, York A, Shroff H, Peckham M. Construction of an instant structured illumination microscope. Methods 2015; 88, 37-47. doi: 10.1016/j.ymeth.2015.07.012.

Ahmed Z, Lin CC, Suen KM, Melo FA, Levitt JA, Suhling K, Ladbury JE. Grb2 controls phosphorylation of FGFR2 by inhibiting receptor kinase and Shp2 phosphatase activity. J Cell Biol. 2013 Feb 18;200(4):493-504. doi: 10.1083/jcb.201204106. PMID: 23420874; PMCID: PMC3575544.

Figure Legends

Figure 1.

Color coded workflow of the 'Cloudbuster' python script. Colors represent the inclusion of python modules in the process: White elements are wxpython module supported, blue are skimage module supported, green elements utilize the numpy module, yellow elements include the Open3D module.

Figure 2.

Representative examples of different point cloud results for data generated by immunohistochemistry. (A) Color coded combination of reconstructed microtome sliced, stained, and scanned images from glioma spheroids using "Meshlab" software. Left to right: red = untreated U251 spheroid grown in medium only, green = Latrunculin A treated U251 spheroid treated with Latrunculin A, blue = U251 spheroid treated with CCG-1423, yellow = BIO treated U251 spheroid. (B) 3D-representation of an U251 spheroid with no treatment and grown in medium only, with green central reference sphere. (C) 3D-representation of U251 spheroid treated with Latrunculin A with green central reference sphere. Note the frazzled appearance of the untreated spheroid compared to the inhibitor treated.

Figure 3.

Comparison of indicators calculated by the 'Cloudbuster' python script. The same color coding as for figure 2 applies: red (medium) = untreated U251 spheroid, green = U251 spheroid treated with Latrunculin A, blue = U251 spheroid treated with CCG-1423, yellow

= U251 spheroid treated with BIO.

(A*) Average point distance to sphere* indicates the average of the accumulated distances of each individual point from the central sphere defined by the minimum dimensional radius of the point cloud. (B) *Fragmentation* of the point cloud calculated by the application of dbscan function of the Open3D module. A size threshold removes potential noise from the calculation. (C) *Y/X extension ratio* of the point cloud binding box measure. The binding box describes the maximum extensions in all dimensions. (D*) Y/Z ratio* of the binding box measure. The value is an indicator of the "flatness" of the spheroid and can also be interpreted as an indicator for the roundness, where a value approaching "1" indicates a perfectly round spheroid if the X/Y ratio also approaches "1". (E) *Number of extensions*. Count of the extensions exceeding the boundaries of a fitted ellipsoid for the central (largest) spheroid. (F) *Average length of extensions*. Average of the outmost vertices derived from the individual extensions identified in µm.

Figure 4.

Representative examples of measurements obtained for data generated from Confocal, ISIM and Lightsheet imaging, respectively. (A) Comparison of two U87 spheroids grown in a collagen matrix for 24 and 48 hours, respectively, and recorded by confocal microscopy. Displayed point clouds were color coded according to the Cloudbuster output and the fitted ellipsoid added in light green. (B) Results excerpt from spheroid quantification. Length data in µm. (C) Point cloud result of ISIM generated tif stack with stained indicative elements. The "meshlab" generated point clouds are coloured to highlight the quantified features: the light green central ellipsoid represents the base for distance/length calculations. Red represents identified extensions from the central ellipsoid. Remaining gray isolated elements represent identified single clouds. (D) The initial point cloud generated from a representative ISIM TIF stack. (E) Excerpt of the quantified features from the point cloud in (D). Size information is shown in µm. (F) Quantification of a Lightsheet TIF stack derived point cloud. The light green central ellipsoid represents the base for distance/length calculations. Red represents identified extensions from the central ellipsoid. (G) initial point cloud from a representative lightsheet TIF stack. (H) The same key indicators as in (E) have been included on the right side. Length data in µm.

Supplemental figures.

Supplemental Figure 1

Preparation of embedded spheroid samples from histochemistry.

(A) Representation of a paraffin block consisting of a collagen embedded U251 spheroid and migratory glioma cells sample.

(B) Representative example of a single spheroid slice on object slide after microtome slicing, clearing and H&E staining.

C) Partial display of semi-automated 5 µm sized scans from a series of single spheroid slices.

Supplemental Figure 2

3D Images of point clouds produced during analysis.

A) Original image stack derived from scanned microtome slices after image spheroid isolation and image registry.

B) Z dimensional linear scaling/interpolation of the original stack resulting in a 1x1x1 (X/Y/Z) dimensional ratio stack.

C) Binary image stack after Li-thresholding of scaled original.

D) Individual point cloud with embedded central reference sphere of treated U251 spheroid treated with the CCG-1423 inhibitor. Point clouds are saved with a ".ply" addition to the original filename.

E) Complementary representation of U251 spheroid treated with BIO inhibitor.

Supplemental Figure 3

Representative screenshots of the graphical user interface for the "Cloudbuster" python script.

A) The initial view after start of the script. Blank entry boxes on the left for the dimensional pixel resolution.

B) View with file selection menu after pressing the "Find stack and start button." Upon confirmation of file selection, the preparation/analysis process will start or show an error message in case the file type could not be identified.

C) Final state after completing processing of loaded image stack. Icons and text in the middle/right part of the windows show the processing steps with the analysis results at the bottom. The single window on the right contains a rotation enabled representation of the resulting point cloud.

Supplemental table 1

Example of a result window and findings generated by Cloudbuster of indicators for the evaluation of 3D microscopical objects, like spheroids. Cloudbuster calculates 24 indicative values from each object.

Figure 1

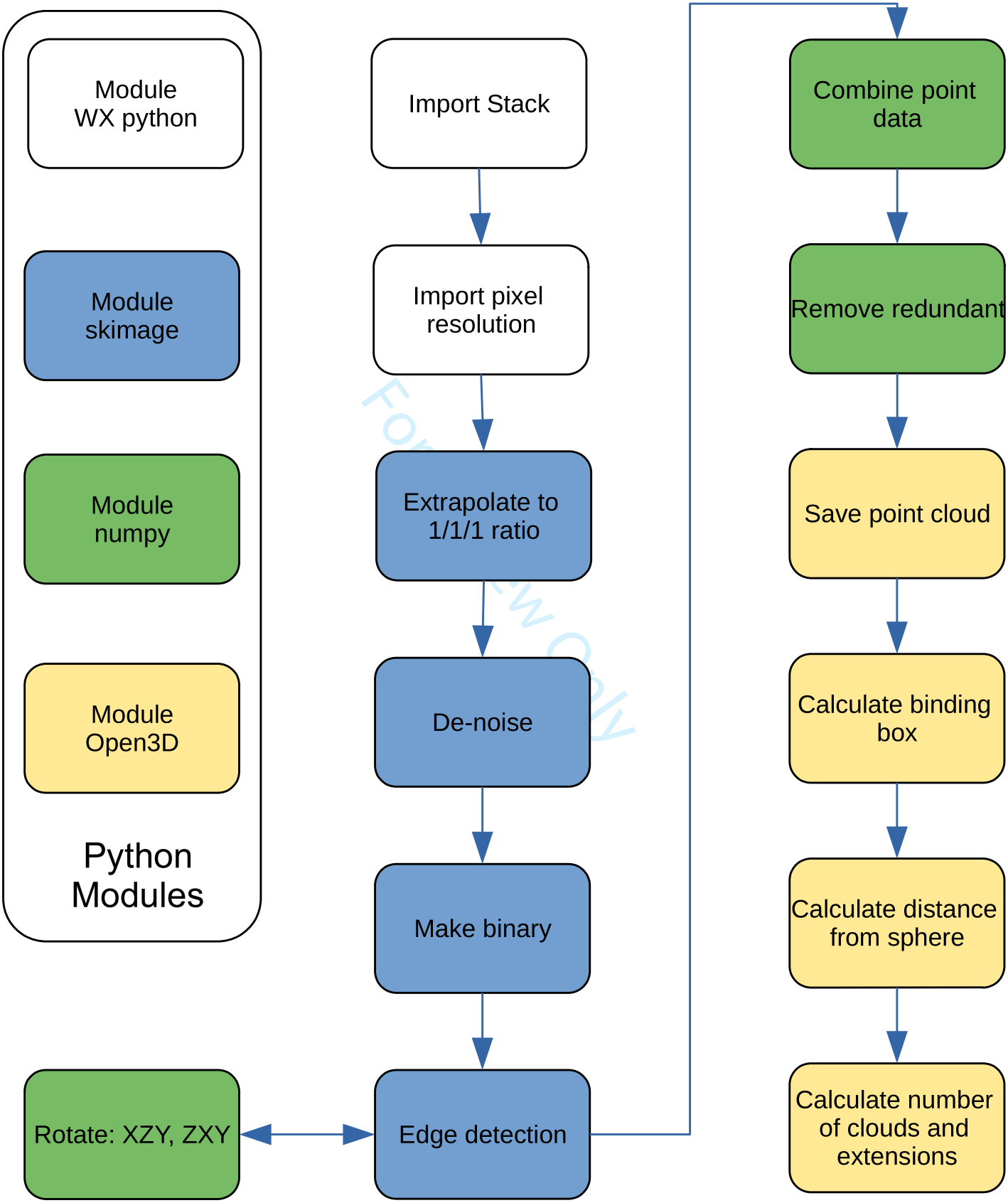

Figure 2

A

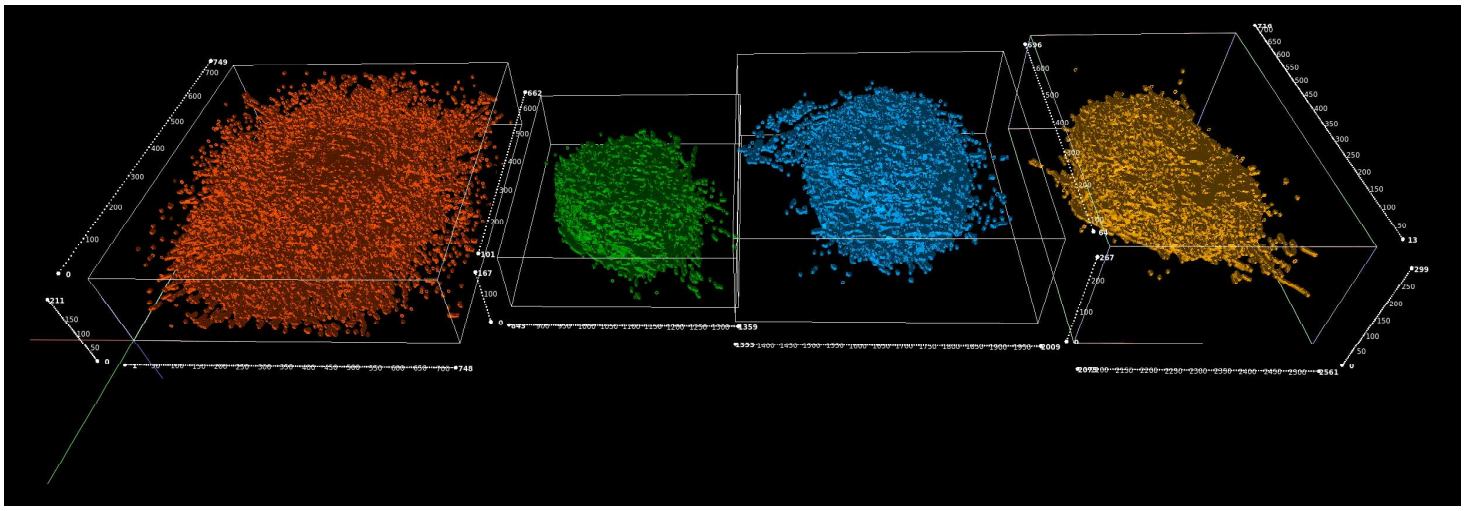

B

Medium

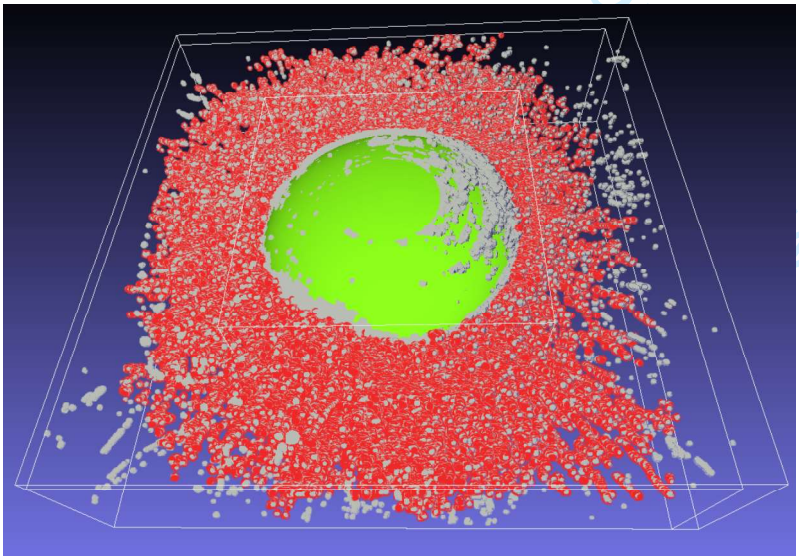

C

Latrunculin A

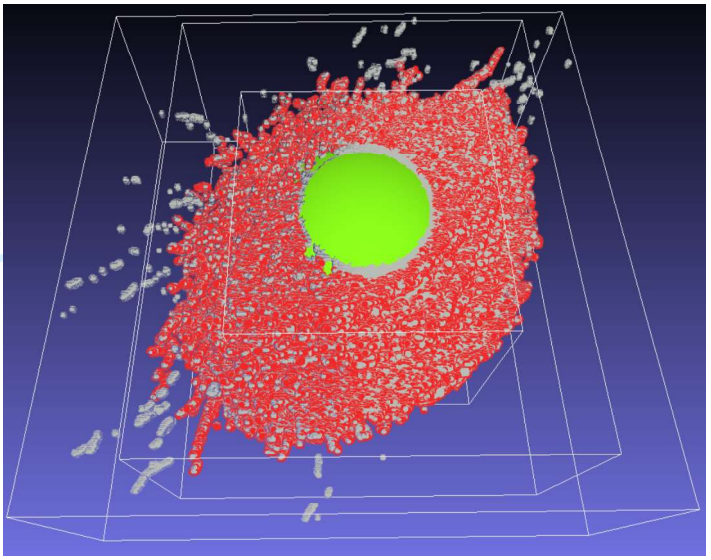

Figure 3

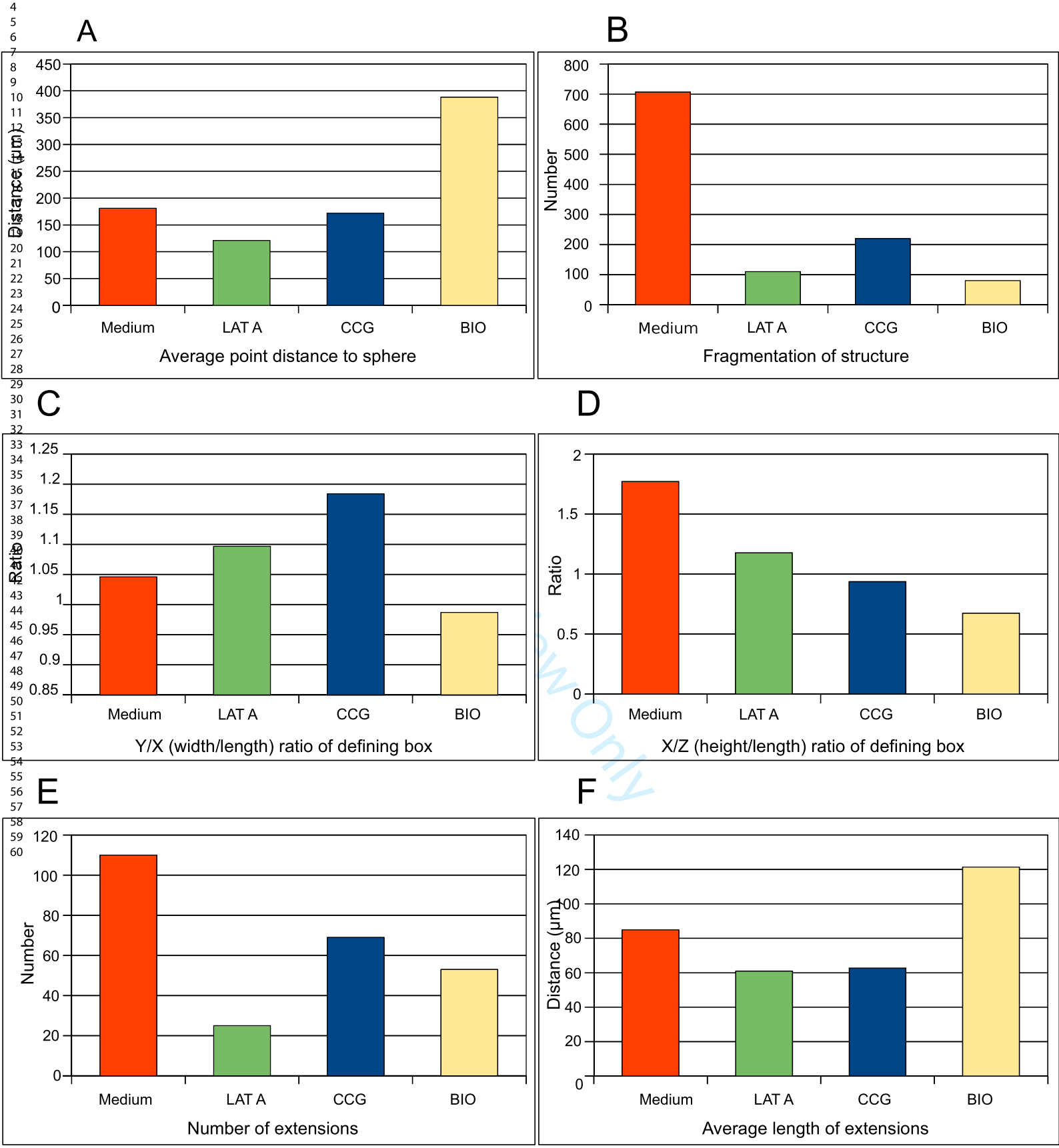

Figure 4

A

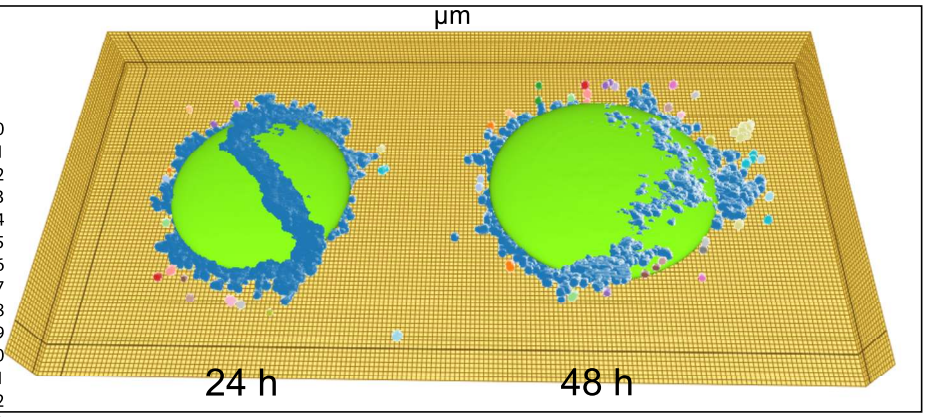

B

	24 h	48 h
Sep. Comp.	17	35
Av. Dist. To Sphere	583.74	623.99
no of ext.	6	11
av. length of ext.	387.16	530.42

C

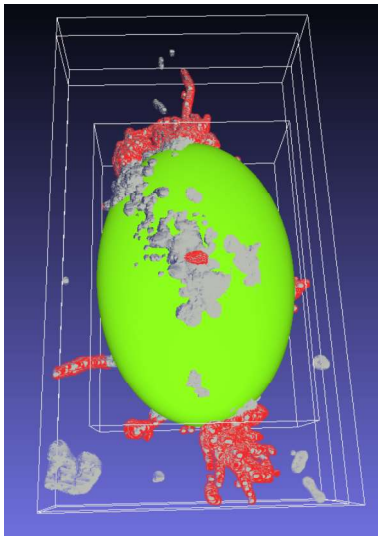

D

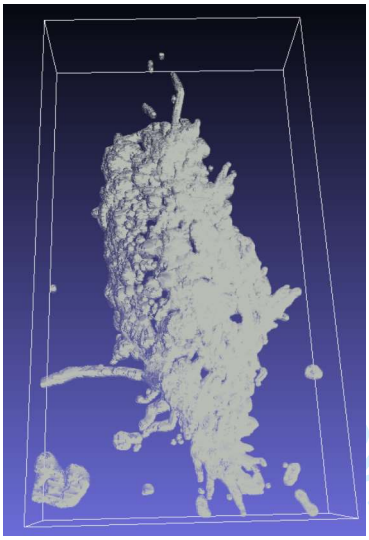

E

Spheroid results

Sep. Comp.	11
Sp. Max. X	8.6961
Sp. Max. Y	13.1269
Sp. Max. Z	3.66
Hint	Spheroid Elongated
Med. Dist.	18.2219
Av. Dist.	16.8508
Var. Dist.	654.4641
Max. Dist.	24.4353

Extension results

No. of Ext.	9
Area (µm²)	176.91
Max. Length	9.29
Av. Length	1.09
Med. Length	1.05
Var. Length	16.40

F

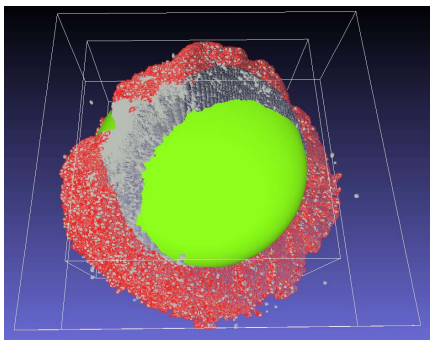

G

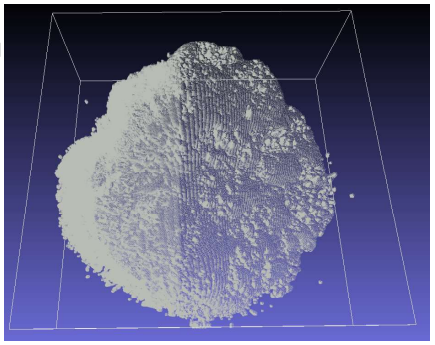

H

Spheroid results

Sep. Comp.	56.00
Sp. Max. X	457.15
Sp. Max. Y	457.15
Sp. Max. Z	212.01
Hint	Spheroid round
Med. Dist.	575.25
Av. Dist.	552.55
Var. Dist.	6196.87
Max. Dist.	706.09

Extension results

No. of Ext.	10.00
Area (µm²)	50077.56
Max. Length	241.87
Av. Length	38.22
Med. Length	37.37
Var. Length	165.89